J Electroceram (2010) 25:188–197
DOI 10.1007/s10832-010-9614-7

# Deep level transient spectroscopy study of the effect of Mn and Bi doping on trap formation in ZnO

**Colin Leach · Karen D. Vernon-Parry · Naheed K. Ali**

Received: 19 November 2009 / Accepted: 28 May 2010 / Published online: 8 June 2010
© Springer Science+Business Media, LLC 2010

**Abstract** Deep Level Transient Spectroscopy (DLTS) characterisation of sintered polycrystalline ZnO, and ZnO doped with Mn, and with Mn plus Bi, has been carried out to investigate the effect of these additions on the formation and activation of electron trap states in ZnO used for varistor applications. Samples were produced using a conventional solid state sintering technique, and sintered at 1100°C and 1200°C, quenching the Bi-free samples from the sintering temperature to preserve high temperature defect distribution and slow cooling the Bi-containing samples to develop varistor behaviour. The two well-known bulk ZnO traps, L1 (0.18 eV below the conduction band edge) and L2 (0.29 eV below the conduction band edge), were observed in both the undoped and doped samples. Detailed characterisation of the L1 and L2 traps indicated that they are due to point defects, since their energy was independent of the length of the fill pulse and the fill bias. The introduction of both 1% Mn and (1% Mn+ 2% Bi) caused several additional electron traps, some of which have not been reported previously, to appear deeper in the band gap with energies depending on composition and firing cycle,. The DLTS peaks associated with these additional traps were very broad and had activation energies that varied with fill pulse length: characteristics that indicate they are associated with extended defects.

**Keywords** DLTS · Zinc oxide · Varistor · Defect · Trap states

C. Leach (✉) · N. K. Ali
School of Materials, University of Manchester,
Manchester M1 7HS, UK
e-mail: colin.leach@manchester.ac.uk

K. D. Vernon-Parry
MERI, Sheffield Hallam University,
Sheffield S1 1WB, UK

## 1 Introduction

ZnO based varistors show non-linear current-voltage behaviour, allowing the passage of a large current only above a threshold level of applied electric field, corresponding to about 3.5 V per grain boundary [1, 2]. The non-linear behaviour is conventionally described in terms of field-dependent current flow across back-to-back double Schottky grain boundary barriers [3, 4], which arise due to band-bending by occupied interface states within the bandgap [5]. The breakdown under high electric field is due to the flow of minority carriers, formed by impact ionisation within the depletion region, which lowers the potential barrier [6]. This behaviour, coupled with the high power handling and low leakage characteristics make varistors suitable for a range of applications including: protection of electronic circuitry, electric power distribution and transmission systems, telecommunications, power engineering and automotive electronics [7].

In order to achieve varistor action, ZnO is doped with a former, such as $Bi_2O_3$ or $Pr_6O_{11}$, which enhances electron trapping by ZnO surface states, and performance enhancing oxides such as MnO, CoO, $Sb_2O_3$ and $Cr_2O_3$ [8]. The role of additives and processing on varistor performance has been described in detail elsewhere [2, 9–11]. $Bi_2O_3$ also promotes liquid-phase sintering [12]. Mn is believed to be distributed homogenously [2] but is electrically active at grain boundaries where it introduces interfacial surface states, acting as a deep donor in ZnO with trap energies 0.7 eV [13], 0.45–0.50 eV [10] and 2.0 eV [14] below the conduction band edge. Increasing Mn additions systematically increase the interface state density [9, 11] pinning the grain boundary potential barrier at low applied fields [15] and giving rise to high non linearity coefficients due to the rapid collapse of the grain boundary barrier by hole-trapping at breakdown [6, 15]. The bulk resistivity of Mn

doped ZnO reduces with increasing sintering temperature in the range 1150–1350°C due to an increase in the concentration of intrinsic donors [16].

The precise form of the I–V characteristic in grain boundary controlled semiconducting ceramics such as varistors and thermistors has been related to the distribution and density of grain boundary interface states [3]. There is therefore a need for experimental data characterising the depth, density, origin and form of such traps in ZnO varistors, and several experimental studies have addressed this [5, 10, 13, 17–30] (Table 1). However the detailed structure and precise role of many of these traps remains unclear.

ICTS (Isothermal Capacitance Transient Spectroscopy) [26] characterisation of interface states in Bi-doped and Pr-doped ZnO varistors identified two defects that were common to both types of varistors, lying 0.61 eV and 0.77 eV below the conduction band edge, and were attributed to adsorbed oxygen. A further trap lying at 0.48 eV below the conduction band edge was also observed in the Bi-doped varistor, and was linked to the formation of spinel phase within the microstructure.

Photo-capacitance spectroscopy [28] and photo-isothermal capacitance transient spectroscopy (photo-ICTS) [23] studies of Pr-doped varistors found evidence for a trap lying 0.9 eV below the conduction band edge, which was attributed to chemisorbed oxygen ions. A direct correlation between the value of the varistor non-linear coefficient and the density of this trap was reported [28].

Several deep level transient spectroscopy (DLTS) [31] studies have identified electron traps in single crystal ZnO [17–19], polycrystalline ZnO [20, 21] and ZnO-based varistors [5, 10, 13, 22–30]. DLTS of single crystal semiconductors is normally performed by observing capacitance changes during the emptying of majority carrier traps at deep states in a depletion region that has been created by applying a reverse bias to a surface Schottky contact. The traps are filled using an externally applied bias (the 'fill pulse'), which is then removed to allow the traps to empty by thermal emission. The emission rate of each peak is measured as a function of temperature, using a series of rate windows, from which it is possible to calculate an energy for the trap, which approximates the trap level with respect

**Table 1** Published data for trap states in single crystal ZnO and polycrystalline ZnO varistors.

| System | Analysis technique | Ea of trap below the conduction band (eV) | Suggested Defect Responsible | Reference |
|---|---|---|---|---|
| Hydrothermal ZnO single crystal | DLTS | 0.30 | $Vo^{o}$ | [17] |
| Proton-bombarded ZnO single crystal | DLTS | 0.12, 0.10±0.02, 0.29, 0.57±0.02 | | [18] |
| Single crystal ZnO | DLTS | 0.12, 0.29, 0.57±0.02 | $V_o$ | [19] |
| ZnO-BaO | DLTS | 0.15, 0.24 | $V_o$ | [20] |
| $ZnO-Bi_2O_3-MnO$ | DLTS | 0.18, 0.27, 0.50, 0.60, 0.89, 1.0 | Point and extended | This study |
| $ZnO-Bi_2O_3$ | ICTS | 0.19, 0.36 | Intrinsic induced by Bi ion, $Zni^{oo}$ and $V_o^{o}$ | [21] |
| $ZnO-Bi_2O_3-MnO$ | ICTS | 0.60 | – | [5] |
| $ZnO-Bi_2O_3-CoO$ | DLTS | 0.14, 0.24 | Intrinsic | [22] |
| $ZnO-Pr6O_{11}-Co_3O_4$ | ICTS | 0.9 | – | [23] |
| Commercial varistor composition | DLTS | 0.17, 0.26, (0.2–0.3) | $Zn_i$ | [24] |
| Commercial varistor composition | DLTS | 0.26 | Doubly ionised Zn interstitial | [9] |
| $ZnO-Bi_2O_3$ | DLTS | 0.98 | – | [25] |
| $ZnO-Bi_2O_3$ and $ZnO-Pr_2O_3$ | ICTS | 0.61, 0.77 in both Bi- and Pr-type | Chemically adsorbed O and $O^{2-}$ | [26] |
| $ZnO-Pr_2O_3$ | ICTS | 0.84 | | [27] |
| $ZnO-Pr_2O_3$ | ICTS single grain boundary measurement | 0.9 | Chemisorbed oxygen ion | [28] |
| Zn-Bi-Co and Zn-Pr-Co-Al | Capacitance transient spectroscopy | 0.6–0.7 | Extrinsic | [8] |
| Commercial varistor composition | DLTS | 0.15, 0.25 | Extrinsic, Zn interstitial | [29] |
| Commercial varistor composition | DLTS | 0.25, 1.1 | – | [30] |
| Commercial varistor composition | Admittance spectroscopy | 0.21, 0.32, 0.17, 0.45–0.50 | Intrinsic | [10] |
| Commercial varistor composition | Admittance spectroscopy | 0.45–0.50 | – | [13] |
| Commercial varistor composition | Admittance spectroscopy | 0.20, 0.32, 0.45–0.50, 0.17 | Intrinsic defects of ZnO | [14] |
| ZnO varistors | Admittance spectroscopy | 0.20, 0.32 | – | [15] |
| ZnO varistors | Admittance spectroscopy | 0.36 | – | [11] |

to the conduction or valence band edge. In analysing DLTS data it is normally assumed that the capture cross-section does not depend on temperature, so the emission rate, $e_n$, is given by:

$$e_n = \sigma_n v_{th} N_c \exp\left(\frac{-\Delta G_n}{kT}\right) \quad (1)$$

and is often simplified to:

$$e_n = \sigma_n v_{th} N_c \exp\left(\frac{E_c - E_T}{kT}\right) \quad (2)$$

where $\sigma_n$ is the capture cross-section, $\nu_{th}$ is the thermal velocity, $N_c$ is the effective density of states in the conduction band and $\Delta G_n$ is the energy needed to excite an electron thermally from a trap into the conduction band, $E_c$ is the position of the conduction band and $E_T$ the energy level of the trap. Equation 2 is normally used to calculate an experimental activation energy, from a plot of ln $(T^2/e_n)$ against 1/T, but the value so obtained is slightly different from the true trap level, as would be calculated from the enthalpy term because the simplifying assumptions ignore the change in entropy associated with electron emission from the trap to the conduction band.

A value for the capture cross-section of the trap can be estimated from the intercept of the plot of ln $(T^2/e_n)$ against 1/T. However, the approximations described above can lead to significant errors in this part of the analysis with calculated capture cross sections varying by up to two orders of magnitude from the true value [32]. Accurate capture cross-sections of traps for majority carriers can be extracted from studies of the capture process rather than the emission process used in DLTS, but since capture times are much shorter than emission times, this can be technically demanding. For this reason we are refraining from presenting calculated values for capture cross-section in this study.

In single crystal materials, the area under the DLTS peak is frequently used to calculate the trap concentration, as the volume probed during the experiment is well-defined. In the case of polycrystalline semiconductors, grain boundary depletion regions are also probed during DLTS, and so it is possible to calculate the level of grain boundary traps (i.e. their position relative to the conduction band (CB) edge for electron traps or relative to the valence band edge for hole traps). However quantification of the defect concentration remains challenging since in real materials the geometry of the depletion regions that are formed under bias cannot be determined accurately. It does however remain possible to make valid judgments about relative trap concentrations in a specific sample by comparing the areas of separate emission peaks within the same spectrum. For example, Fan and Freer [29] studied the effect of Ag and Al doping on the I–V characteristics of a varistor. They found two electron traps at 0.15±0.01 eV and 0.25±0.01 eV below the conduction band in both compositions, and reported that Al doping increases the trap density, donor density and α, whereas Ag doping had the opposite effect. Rohgati et al. [24] found a decrease in the density of the trap at 0.26 eV below the conduction band after annealing at 600°C and suggested that the density of this trap is related to varistor stability.

Although DLTS studies have been performed on several commercial varistor formulations [24, 25, 29, 30], these generally contain several additives in differing proportions and are sintered over a range of temperatures. Consequently comparison of the data is difficult and the specific effect of each additive on trap formation has not yet been established with certainty. In addition the fine-scale structures of the traps that have been identified have not been studied in detail.

In this study we have used DLTS to characterise the effects of Mn doping and variations in sintering temperature on trap development in ZnO. We have achieved this by comparing trap densities and distributions in undoped and Mn-doped polycrystalline ZnO that has been sintered at two temperatures. We have specifically investigated the interaction of Mn with Bi in order to investigate the effect of Bi on the formation, activation and development of these (Mn induced) trap states in simple varistor structures. In addition we have carried out a novel detailed study of the structure of the electron traps present in one sample (Mn doped ZnO sintered at 1100°C), to establish which states are associated with (intrinsic or extrinsic) point defects, and which are associated with extended defects, by characterizing variations in apparent activation energy with fill pulse and capture cross-section.

## 2 Experimental procedure

ZnO (99.99% purity), ZnO doped with 1 mol.% Mn (as carbonate) and ZnO doped with 1 mol.% Mn and 2 mol.% Bi (as oxide) powders were prepared via a standard mixed-oxide route by weighing, ball-milling and calcining at 500°C for 5 h. 4 mm thick pellets, 10 mm in diameter, were pressed, and sintered at 1100°C or 1200°C for 2 h. The samples so produced are referred to here as Z-1100, Z-1200, ZM-1100, ZM-1200 and ZMB-1200, according to composition and sintering temperature. The Z- and ZM- samples were air quenched from the sintering temperature in order to minimize the effects of oxygen diffusion during cooling and allow the effect of Mn on the defect chemistry of ZnO to be investigated as a function of sintering temperature. Sample ZMB-1200 was required to show varistor behaviour and so was cooled from the sintering temperature at a rate of 2°C $min^{-1}$, allowing grain boundary electrical barriers to develop so that the trap

structures associated with Mn and Bi additions in ZnO based varistors could be characterised.

The sintered pellets were prepared for microstructural characterisation by polishing with diamond paste and a colloidal silica suspension. Backscattered (BS) electron images were captured using a JEOL 6300 SEM with EDX facility. Grain size was measured using the linear intercept method and densities were established using the Archimedes' method. Bulk electrical measurements were made using In-Ga paste electrodes and a custom test rig.

For DLTS measurements, the sintered pellets were ground to a thickness of 1 mm and polished on both sides. An array of 1 mm diameter Ohmic, Au top contacts was deposited onto one polished face and a second, Ohmic, Au back-electrode deposited onto the opposite face. Each sample was mounted on an insulating ceramic substrate, with electrical contact made through wires bonded to one top contact and the back electrode (Fig. 1). An electric field was applied across the specimen, which modified the size of the grain boundary depletion regions below the top electrode. Since the contacts were Ohmic, no Schottky barrier depletion region was created below the electrode and therefore the resultant signal was localised to the grain boundary depletion regions. The emission rate was measured as a function of temperature for each sample and the energy of each trap established from the variation of peak emission rate for each rate window with temperature. In the subsequent discussion it is assumed that all grain boundary depletion regions perpendicular to the electric field and directly under the contacts were activated for the DLTS measurements.

## 3 Results

### 3.1 Microstructure

Figure 2(a–e) shows BS images of each of the samples. Table 2 lists the corresponding specimen densities and grain sizes. Samples Z-1100 (Fig. 2(a)) and Z-1200 (Fig. 2(b)) are almost fully dense, with similar grain sizes and only a few small pores at triple points. The addition of Mn in samples ZM-1100 (Fig. 2(c)) and ZM-1200 (Fig. 2(d)) has slightly reduced both the mean grain size and the sample density. The addition of excess Bi and Mn (sample ZMB-1200: Fig. 2(e)) has led to the formation of a Bi-rich phase, which has pooled at triple junctions and penetrated as a thick film along many grain boundaries, rounding the grains and increasing the mean grain size due to liquid phase sintering. A few large pores remain. The Bi-rich film in sample ZM-1200 contained 0.4–0.5 mol.% of dissolved Mn-ions, elsewhere the Mn was found to be uniformly distributed within the ZnO grains and at grain boundaries in all samples, within the limits of EDX analysis.

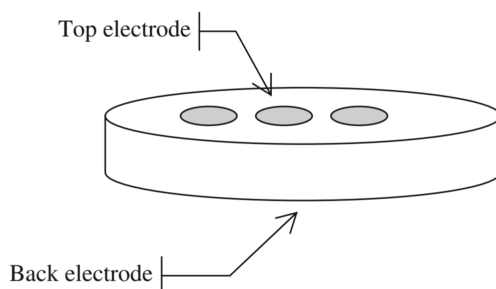


**Fig. 1** Schematic diagram showing the electrode configuration for DLTS

Samples Z-1100 and Z-1200 both showed Ohmic I–V behaviour with a resistivity of 400Ω cm. The addition of Mn increased the resistivity to $6\text{x}10^7$ Ω cm (ZM-1100) and $3.4\times10^3$ Ω cm (ZM-1200) respectively. Sample ZMB-1200 showed varistor behaviour with a non-linearity coefficient of 9 and a leakage current, measured at 70% of the breakdown voltage, of 13 μA $\text{cm}^{-2}$.

### 3.2 Deep level transient spectroscopy

The fill pulse, applied between the back-electrode and one 1 mm diameter top electrode, was assumed to affect all grain boundaries below the top electrode equally, averaging the effects of variations in the size of the depletion region due to microstructural or structural differences between grain boundaries. The DLTS information so obtained was considered to represent a 'typical' grain boundary, based on all the grain boundary structures present within the measured region.

Since the width and total area of the active depletion regions could not be determined accurately, it was not possible to make quantitative measurements of trap density, and so the measurement conditions that were used were based on achieving a good signal-to-noise ratio with spectral reproducibility. As a result measurement conditions of a−10 V bias, 20 ms long fill pulse, and a 0 V measurement bias were adopted for all samples apart from ZM-1200 where a fill pulse of 0.1 V for 2 ms, and a measurement bias of −3 V were used. The voltage per grain boundary experienced by each sample during measurement therefore varied slightly according to sample thickness and grain size, although it was confirmed in each case that full trap activation had taken place. Except where stated otherwise, spectra obtained at an emission rate of 200 $\text{s}^{-1}$ were used to compare DLTS peak areas. All traps were found, from the polarity of the DLTS signal, to be electron traps and so analysis of the variation of emission with temperature gave the energy of the trap below the conduction band edge (Ea).

Table 3 summarises DLTS data for each sample. The well-known L1 trap [27], at Ea=0.18±0.02 eV, was observed in

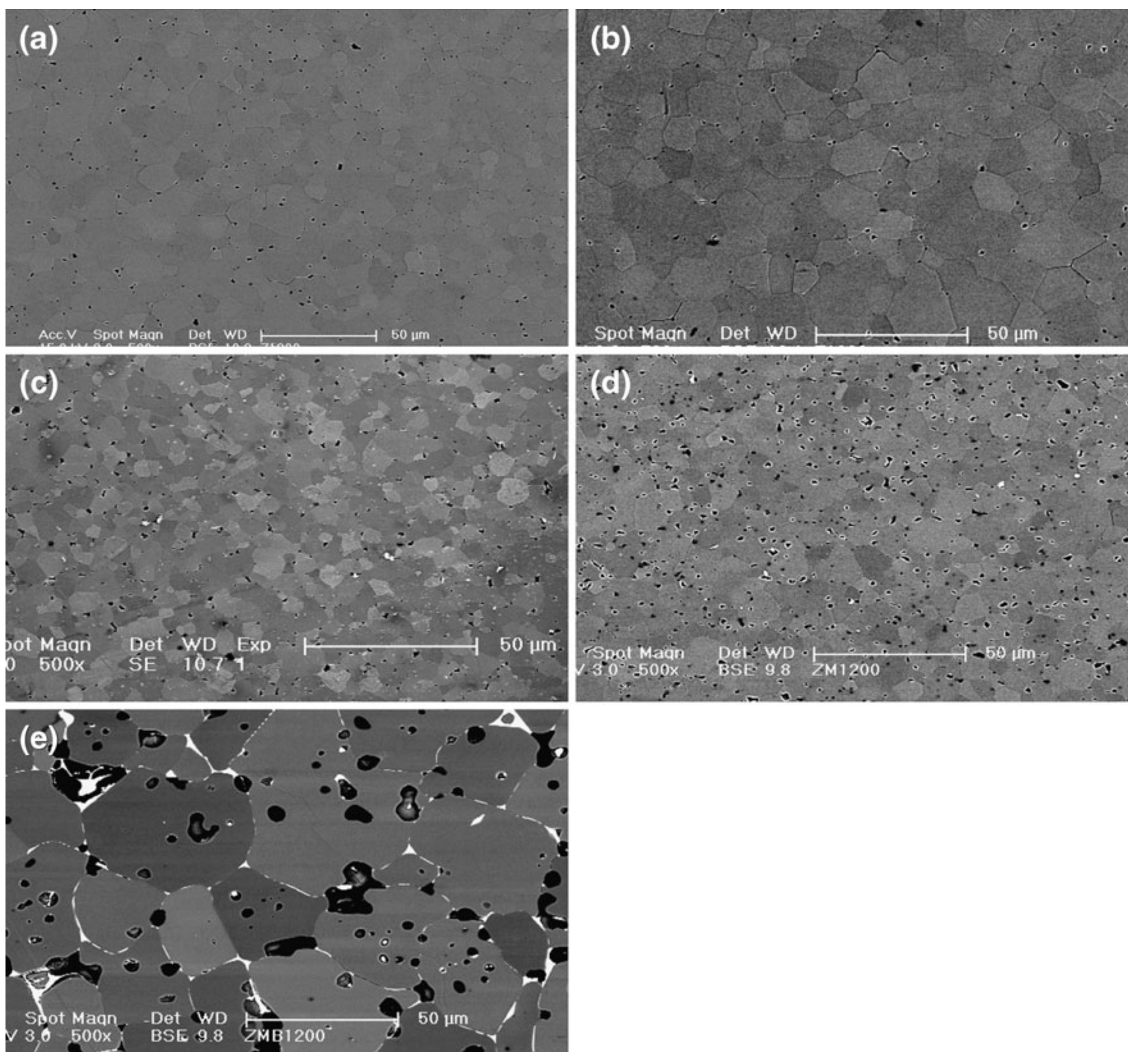


**Fig. 2** BS images of samples (**a**) Z-1100, (**b**) Z-1200, (**c**) ZM-1100, (**d**) ZM-1200, and (**e**) ZMB-1200

all samples except Z-1100. This indicates that in undoped ZnO a sintering temperature in excess of 1100°C is necessary to activate this defect. The peak at Ea=0.29±0.02 eV, corresponding to the previously reported L2 trap [29], was found in all samples, and was independent of dopant(s) and sintering temperature over the range studied here. A trap at Ea=0.50±0.03 eV was also observed in the undoped ZnO samples.

**Table 2** Densities and grain sizes of the samples prepared for this study.

| Sample | Relative density (%) | Grain size (µm) |
|---|---|---|
| Z-1100 | 99 | 20±3 |
| Z-1200 | 99 | 21±4 |
| ZM-1100 | 93 | 12±1 |
| ZM-1200 | 95 | 16±4 |
| ZMB-1200 | 85 | 28±4 |

The addition of 1 mol.% Mn to the ZnO suppressed the trap at Ea=0.50±0.03 eV, but resulted in the formation or activation of two additional electron traps at Ea=0.60±0.03 eV and Ea=1.0±0.1 eV in sample ZM-1100 and one trap at Ea=0.89±0.05 eV in sample ZM-1200.

Whilst the L1 and L2 traps are still present in sample ZMB-1200, all of the deeper traps that were found in samples ZM-1100 and ZM-1200 have disappeared, and are replaced by a broad peak corresponding to a trap at Ea=0.45±0 .02 eV.

Figure 3(a–e) shows the DLTS spectra from the samples, for an emission rate of 200 $s^{-1}$. In sample Z-1100 (Fig. 3(a)) there are two peaks of approximately the same area (and hence associated with traps of approximately the same concentration). These peaks correspond to L2 at 188 K and a trap with Ea=0.50 eV at 257 K. In sample Z-1200 (Fig. 3(b)), both these peaks are again present, but are joined by a third, much larger, peak at 138 K, which is attributed to the L1 defect. In the spectra from samples ZM-1100

**Table 3** Trap energies for all samples calculated from DLTS data at an emission rate of 200 $s^{-1}$.

| Sample | T(K) | Ea (eV) | T (K) | Ea (eV) | T(K) | Ea (eV) | T(K) | Ea (eV) | T(K) | Ea (eV) | Temp. range of measurement (K) | Fill time (ms) |
|---|---|---|---|---|---|---|---|---|---|---|---|---|
| Z-1100 | – | – | 188 | 0.29±0.02 | 258 | 0.49±0.03 | – | – | – | – | 80–300 | 20 |
| Z-1200 | 138 | 0.18±0.01 | 184 | 0.27±0.02 | 257 | 0.50±0.03 | – | – | – | – | 80–300 | 20 |
| ZM-1100 | 135 | 0.19±0.01 | 189 | 0.29±0.01 | – | – | 355 | 0.60±0.03 | 385 | 1.0±0.1 | 80–400 | 20 |
| ZM-1200 | 134 | 0.19±0.01 | 188 | 0.30±0.01 | – | – | 311 | 0.89±0.05 | – | – | 80–350 | 2 |
| ZMB-1200 | 135 | 0.16±0.02 | 182 | 0.27±0.02 | – | – | – | – | 382 | 0.45±0.02 | 80–400 | 20 |

(Fig. 3(c)) and ZM-1200 (Fig. 3(d)), the addition of Mn has decreased the area of the L1 peak relative to L2, and hence the relative trap density. The peak observed in undoped ZnO at 258 K has been suppressed and new peaks have appeared in the range 300–350 K. The two, new, high temperature peaks in sample ZM-1100 were poorly resolved at a rate window of 200 $s^{-1}$ and so an additional curve, corresponding to a rate window of 80 $s^{-1}$ is also shown for clarity. In sample ZMB-1200 (Fig. 3(e)) the L1 peak is now reduced to half the area of L2, further reducing the ratio of trap densities. The higher temperature peaks, visible in the other samples, are also replaced by another with lower Ea. While the positions and energies of the L1 and L2 peaks remain fixed in all samples the higher temperature peaks show considerable variation between samples, suggesting that their formation and stabilisation is very sensitive to both local composition and structure variations induced by differences in processing.

### 3.3 Trap structure studies

Sample ZM-1100 was selected for detailed study, and so the fine structures of the traps present in this sample were characterised by considering the effects of fill pulse length and fill bias voltage on measured trap depth, Ea. The same electrode contacts were used for all measurements within this study, maintaining a constant sample geometry and ensuring the same grain boundaries were activated under each set of measurement conditions. This sample has a mean grain size of 12μm and so, based on a simple brick-layer model and a sample thickness of 1 mm, the average voltage per grain boundary for each measurement would be approximately 1/80 of the overall applied voltage.

Figure 4 shows DLTS spectra of ZM-1100 showing the L1 and L2 peaks, and peak 3, collected at an emission rate of 200 $s^{-1}$, for different conditions of fill bias and pulse length. The temperature and relative concentration of the L1 and L2 peaks show little variation under these differing conditions, which implies they behave as isolated point defects within the analysed volume. Their energies are not affected by strain field of grain boundaries, as can be seen when a low fill bias (−3 V) is used, limiting the analyses area to the immediate proximity of the grain boundary.

Peak 3, however, varies in peak temperature and area according to the measurement conditions. Its concentration relative to L1 and L2 clearly depends on fill pulse length and the volume of material probed on either side of the grain boundary (fill voltage). Whilst the difference between the defect concentration measured with −10 V and −5 V fill biases is only slight, the drop in concentration for −3 V is significant, suggesting that the highest density of defect responsible exists slightly away from the exact grain boundary plane.

For the L1 and L2 traps values of Ea were found to be unaffected by changes in fill bias voltages in the range 0 V to −5 V, measurement bias in the range −10 V to 0 V, and fill times in the range 20 ms to 0.05 ms (Table 4). However, the traps, nominally at Ea=0.60±0.02 eV (peak 3) and at Ea=1.0±0.1 eV (peak 4) both show significant variation in apparent Ea with fill pulse length and voltage (Table 5), indicating that the emission rate into the various rate windows is affected by the charge state of the defect.

The activation energy of a well-behaved isolated point defect is independent of fill pulse duration, but an extended defect structure will charge up during the fill pulse and change the local band bending. This gives rise to variations both in Ea and the capture cross-section (σ) of the defect [33]. Thus electron capture into an extended defect causes a Coulombic barrier to evolve with time, and the DLTS signal will therefore show dependence on the fill pulse time ($t_F$) according to [34]:

$$n_T(t_F) = \sigma v_{th} n \tau N_T \ln(t_F/\tau) \quad (3)$$

where $n_T(t_F)$ is the time dependent trap occupancy, n the carrier concentration, $v_{th}$ the thermal velocity, $N_T$ the trap concentration, $t_F$ the fill pulse duration and τ a measure of the time required for the trapped charge to begin to affect the Coulombic barrier. Whilst the L1 and L2 traps show the characteristic behaviour of isolated point defects, peaks 3 and 4 behave in a manner characteristic of extended defects.

## 4 Discussion

The L1 electron trap at Ea=0.17±0.02 eV was observed in all of our samples except Z-1100 and is widely reported in

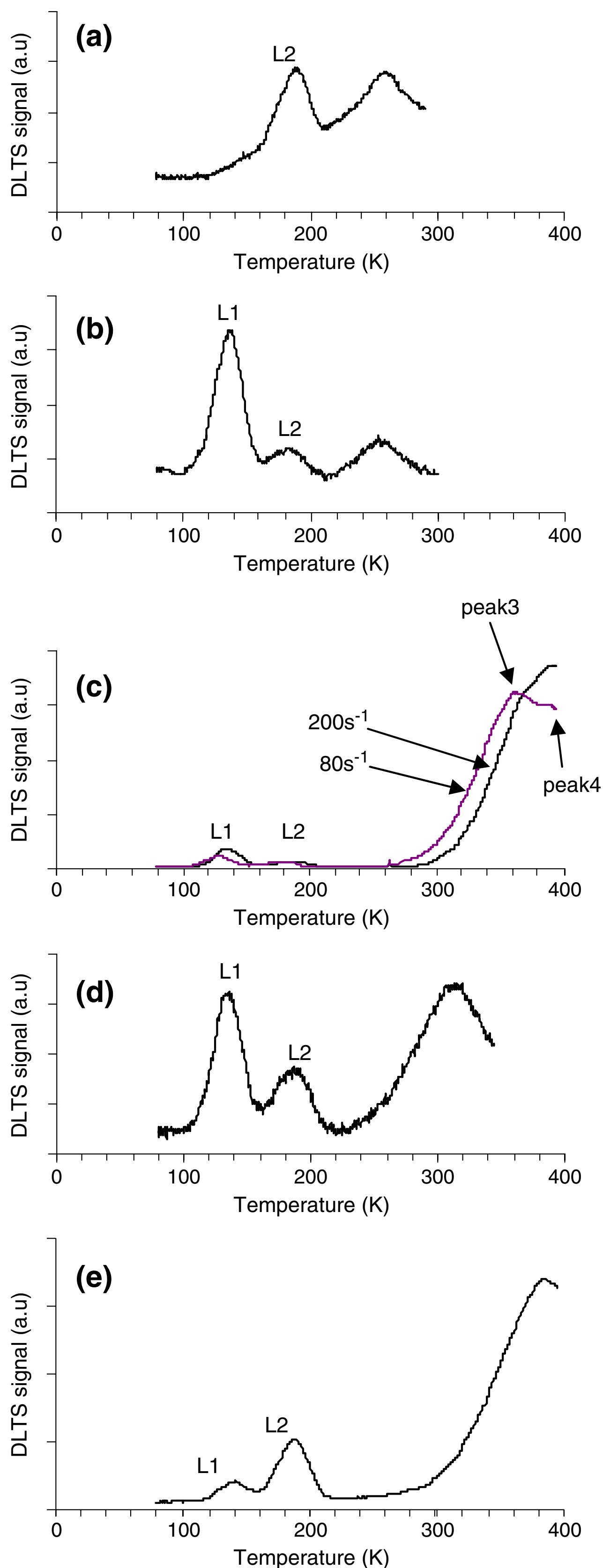


**Fig. 3** DLTS spectra (for an emission rate of 200 $s^{-1}$) (**a**) Z-1100, (**b**) Z-1200, (**c**) ZM-1100 with additional curve for an emission rate of 80 $s^{-1}$: (in this case peaks 3 and 4 are indicated according to the nomenclature in Tables 4 and 5), (**d**) ZM-1200 and (**e**) ZMB-1200. Corresponding activation energies for each temperature of peak are listed in Table 3

DLTS studies of polycrystalline ZnO and ZnO-based varistors [20, 22, 24, 29]. The same trap has been observed in the ZnO–$Bi_2O_3$ system by ICTS (Ea=0.19 eV) [21] and admittance spectroscopy (Ea=0.17 eV) [10]. The precise structure of this trap is currently unclear although it has been suggested that it may be associated with an extrinsic donor defect [29]. This suggestion does not, however, explain why the trap occurs at the same energy when different dopant species are incorporated. The sharpness and symmetrical shape of the L1 peak in each sample (Fig. 3) is more consistent with it being due to an isolated point defect, as is the constancy of Ea (Table 4) as a function of the fill bias voltage and pulse length.

The L2 defect, with Ea=0.29±0.02 eV, which was observed in all our samples, has been reported to occur both in single crystal ZnO [17–19] and polycrystalline ZnO [22, 24, 29, 30]. The exact nature of this defect is also unknown; although it has been suggested that it is associated with a structural defect or impurity within bulk native ZnO [19]. However, the sharpness and symmetrical shape of the DLTS peak in each sample, coupled with our data showing the invariance in Ea with fill time or pulse length, suggests that it, too, is due to an isolated point defect.

The lack of variation of Ea with fill voltage and fill pulse length for the L1 and L2 defects suggests not only that these electron traps are due to point defects, but also that they exist both very close to the grain boundaries and deeper within the grains in essentially the same form. This is because the same defect peaks with the same characteristics are found in DLTS spectra for all values of the depletion width (within the bias range used) and filling density (pulse length). The energies of these defects are

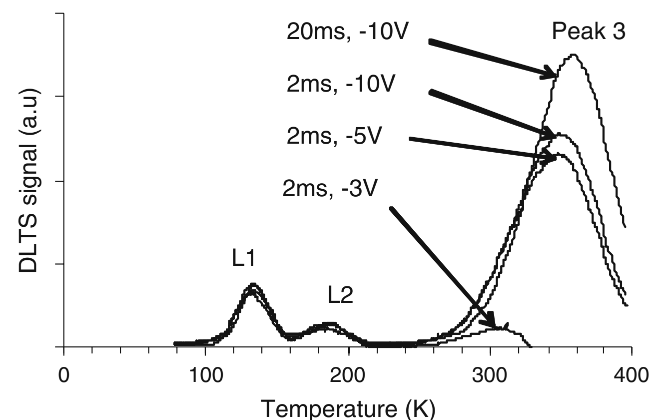


**Fig. 4** DLTS spectra of sample ZM-1100 under different experimental conditions

**Table 4** Variation in Ea for the L1 and L2 peaks in sample ZM-1100 with fill bias and fill length.

| Fill pulse length (ms) | Fill bias (V) | Measurement bias (V) | L1 Peak Ea (eV) | L2 Peak Ea (eV) |
|---|---|---|---|---|
| 20 | −10 | 0 | 0.18 | 0.29 |
| 10 | −10 | 0 | 0.17 | |
| 5 | −10 | 0 | 0.17 | |
| 2 | −10 | 0 | 0.17 | 0.29 |
| 1 | −10 | 0 | 0.17 | |
| 0.5 | −10 | 0 | 0.16 | |
| 0.2 | −10 | 0 | 0.16 | |
| 0.1 | −10 | 0 | 0.17 | |
| 0.05 | −10 | 0 | 0.17 | |
| 2 | −3 | 0.1 | 0.16 | 0.28 |
| 2 | 0 | −5 | 0.15 | 0.28 |

therefore unaffected by any localised strain field at the grain boundaries. Our attribution of L1 and L2 to intrinsic point defects also explains why such good agreement is found in the literature for the properties of these defects in samples prepared under different sintering conditions, and with significant differences in doping level and species.

The peak with Ea=0.49 eV, observed in samples Z-1100 and Z-1200, may correspond to the 'so-called' E4 defect which has been reported in single crystal ZnO [19]. A peak with a similar Ea (0.50 eV) has previously been attributed to a singly ionized oxygen vacancy [17]. Admittance spectroscopy studies identified a defect with Ea in the range 0.45–0.50 eV in commercial ZnO varistors prepared using various additives and heat treatments [10, 13]. Its persistence over a wide range of compositions and preparation routes is, however, consistent with the trap being due to an intrinsic defect. Both of the traps that are observed in sample Z-1100, at Ea=0.29±0.02 eV (L2) and Ea=0.49±0.03 eV, have been reported in single-crystal material [18, 19], and so no electrically active defects solely associated with the grain boundary structure are necessarily present in this sample.

According to the DLTS peak areas, the ratio of the densities of these two defects in samples Z-1100 and Z-1200 lies midway between that reported for freshly annealed single crystal ZnO [19], where the Ea=0.49 eV peak is much smaller than L2, and that observed in proton-irradiated single crystal material, where it is the dominant defect [18]. Additionally, we note that the area of the Ea=0.49 eV peak, relative to L2, in our samples is slightly increased at the higher sintering temperature (Fig. 3(a,b)). On this basis the relative concentration of the 0.49 eV trap could reflect an increasing defect density in the lattice, and is certainly consistent with being associated with vacancies, possibly oxygen as previously suggested, since the defect concentration would be increased by raising the sintering temperature or by proton irradiation.

The loss of the peak at Ea=0.49±0.03 eV when 1 mol% Mn is added to ZnO (samples ZM-1100 and ZM-1200) highlights the instability of the associated defect structure in the presence of Mn. Although little supporting data exists in the literature, a related electrical conductivity study of undoped and Mn doped ZnO [14] showed that Mn addition progressively decreased electron mobility. Such behaviour would also reflect a change in the environment of specific defects that might be observed as shifts in, or passivation of, the DLTS signal.

The trap formed with Ea=0.60±0.03 eV in sample ZM-1100 is at the same level as a trap that has been reported previously within Bi-doped [5] and Pr-doped varistors [26], although its nature has not been identified. The DLTS peak appears quite broad (Fig. 3(d)), which suggests it has a structure more complex than that of a single isolated point defect. Our detailed characterisation, showing the strong variation of activation energy with applied bias and fill pulse duration (Table 5 – peak 3), strongly suggests that this trap is caused by an extended defect. This is because increasing the bias during the fill pulse will widen the depletion region and hence sample a volume extending further into the grain from

**Table 5** Variation in Ea for the higher temperature emission peaks (labelled 3 and 4 in Fig. 3(c)) in sample ZM-1100 with fill bias and fill length.

| Fill pulse length (ms) | Fill bias (V) | Measurement bias (V) | Peak 3 Ea (eV) | Peak 4 Ea (eV) |
|---|---|---|---|---|
| 20 | −10 | 0 | 0.63±0.02 | 1.0±0.1 |
| 2 | −10 | 0 | 0.64±0.01 | 0.78±0.03 |
| 2 | −3 | 0 | 0.89±0.05 | – |
| 2 | −5 | 0 | 0.57±0.02 | – |
| 0.2 | −10 | 0 | 0.77±0.03 | 1.2±0.1 |

the grain boundary. The change in activation energy with bias is interpreted as being due to a progressive change in the local environment, and hence energy, of the defect away from the grain boundary. The change with fill pulse is similar. Further, as more defect sites become occupied and charged, distortions to the local band bending also occur, changing the energy range of the defect.

Similarly, the strong variation in activation energy with fill pulse length and time of the broad peak corresponding to the previously unreported defect with Ea=1.0 eV (Table 5 – peak 4) suggest that this too is due to a defect with a changes slightly in structure as it extends away from the grain boundary. It is not clear from our measurements whether these extended defects lie within, or are simply located adjacent to, the grain boundaries. However they must be contained within the width of the depletion region created in the vicinity of the grain boundaries by the application of a reverse bias, and since they are observed even at the lowest biases it is clear they are primarily located close to the grain boundary. The different rates of change of activation energy for these two high-temperature traps are attributed to differences in the sensitivity of the energy variation to local environment and fill rate of these particular defects: subtle differences in local strain fields caused by the defects and the amount of Coulombic repulsion built up at the defects by carrier capture will result in differences in response of the experimental activation energy to changes in fill pulse length.

The high temperature traps, present in the ZM samples, have all disappeared in ZMB-1200. Thus the combination of a 2% Bi addition and a slower cooling rate has either deactivated them or suppressed their formation. This observation adds further support to the suggestion that these levels are due to extended defect states, since these are more likely (than point defects) to be affected by the changes in the grain boundary structure introduced by the addition of bismuth, or the change in cooling rate.

A previously unreported shallow, high temperature trap at Ea=0.45±0.02 eV has also formed in ZMB-1200. The energy of the trap lies close to the trap measured in Z-1100 and Z-1200, but is distinct in that the peak emission characteristics are different. The associated peak is relatively broad (Fig. 3(e)), which is again consistent with being associated with a defect more complex than a single, isolated point defect. This peak is much larger than those associated with the L1 and L2 defects, indicating either a significantly larger capture cross-section or greater trap density.

## 5 Conclusions

DLTS has been used to characterise trap formation and structure in polycrystalline ZnO sintered at 1100°C and 1200°C, both undoped and with additions of either 1 mol.% Mn, or 1 mol.% Mn+2 mol.% Bi. The undoped and Mn containing samples were quenched from the sintering temperature to preserve the high temperature defect structure and the Mn plus Bi containing sample was slow cooled to allow varistor behaviour to develop.

It was found that increasing the sintering temperature of undoped ZnO from 1100°C to 1200°C activated the L1 defect whilst keeping the two defects found in the Z-1100 sample: namely the L2 defect and the trap at Ea=0.50 eV. The addition of 1 mol.% Mn introduced or activated the L1 defect in the 1100°C sintered sample, but also removed the trap at Ea=0.50 eV, while introducing new electron traps at Ea=0.60 eV and Ea=1.0 eV. The addition of 2 mol.% Bi to the Mn-doped sample sintered at 1200°C removes or passivates all the observed defects except L1 and L2 and introduces one new level with Ea=0.45 eV. The traps at 1.0 eV and 0.45 eV have not been reported previously.

Detailed fill pulse length studies of traps in Mn-doped ZnO have been reported for the first time. The invariance of activation energy and peak temperature of the L1 and L2 defects with measurement conditions indicate that they are due to point defects, and that they occur very close to, or within the grain boundaries. The L1 trap has been attributed to an intrinsic defect (rather than a dopant as was previously reported). The other high temperature peaks found in the sample showed a systematic variation of Ea with measurement conditions and were attributed to electrically active, extended defects.

Comparison of the DLTS peak shapes for the other samples in this study suggest that only the L1 and L2 traps are due to single, isolated point defects, and that other peaks are associated with more complex defects, possibly associated with structural disorder at, or near, the grain boundaries. The exact nature of these more complex traps, including their depth and, where more than one appears in the same sample, their relative density, depends on the sintering conditions and dopant additions.

## References


1. M. Matsuoka, Non-ohmic properties of zinc oxide ceramics. Jpn. J. Appl. Phys. **10**, 736–746 (1971)
2. D.R. Clark, Varistor ceramics. J. Amer. Ceram. Soc. **82**, 485–502 (1999)
3. G.E. Pike, C.H. Seager, The dc voltage dependence of semiconductor grain boundary resistance. J. Appl. Phys. **50**, 3414–3422 (1979)
4. G.E. Pike, S.R. Kurtz, P.L. Gourley, H.R. Philipp, L.M. Levinson, Electroluminescence in ZnO varistors: Evidence for hole contributions to the breakdown mechanism. J. Appl. Phys. **57**(12), 5512–5518 (1985)
5. T. Maeda, S. Meguro, M. Takata, Isothermal capacitance transient spectroscopy in ZnO varistor. Jpn. J. Appl. Phys. **28**, L714–716 (1989)

6. G.E. Pike, Electronic properties of ZnO varistors: A new model. Mater. Res. Soc. Symp. Proc. **5**, 369–379 (1982)
7. R. Puyane, Application and product development in varistor technology. J. Mater. Process. Technol. **55**, 268–277 (1995)
8. J.P. Gambino, W.D. Kingery, G.E. Pike, H.R. Phillip, L.M. Levinson, Grain boundary electronic states in some simple ZnO varistors. J. Appl. Phys. **61**(7), 2571–2574 (1987)
9. T.K. Gupta, Application of ZnO varistors. J. Am. Ceram. Soc. **73**, 1817–1840 (1990)
10. F. Greuter, G. Blatter, Electrical properties of grain boundaries in polycrystalline compound semiconductors. Semicond. Sci. Technol. **5**, 111–137 (1990)
11. L.M. Levinson, H.R. Philipp, Zinc oxide varistors—a review. Bull. Am. Ceram. Soc. **65**, 639–646 (1986)
12. H. Wang, Y.M. Chiang, Thermodynamic stability of intergranular amorphous films in bismuth doped ZnO. J. Am. Ceram. Soc. **81** (1), 89–96 (1998)
13. R. Einzinger, Grain boundary phenomena in ZnO varistors In Grain boundaries in semiconductors. Mater. Res. Soc. Symp. Proc., ed. by H.J. Leamy, G.E. Pike and C.H. Seager (Elsevier New York 1982) pp 343–355
14. J. Han, P.Q. Mantas, A.M.R. Senos, Defect chemistry and electrical characterisation of undoped and Mn-doped ZnO. J. Europ. Ceram. Soc. **22**, 49–59 (2002)
15. M. Rossinelli, F. Greuter, F. Schmuckle, Electrically active grain boundaries in ceramics: Varistors and capacitors. Br. Ceram. Proc. **41**, 177–188 (1989)
16. S.-N. Bai, T.-Y. Tseng, Influence of sintering temperature on electrical properties of ZnO varistors. J. Appl. Phys. **74**, 695–703 (1993)
17. J.C. Simpson, J.F. Cordaro, Characterisation of deep levels in zinc oxide. J. Appl. Phys. **63**, 1781–1783 (1988)
18. F.D. Auret, S.A. Goodman, M. Hayes, M.J. Legodi, H.A. Van Laarhoven, D.C. Look, Electrical characterisation of 1.8 MeV proton-bombarded ZnO. Appl. Phys. Lett. **79**, 3074–3076 (2001)
19. F.D. Auret, S.A. Goodman, M.J. Legodi, W.E. Meyer, D.C. Look, Electrical characterisation of vapour-phase-grown single-crystal ZnO. Appl. Phys. Lett. **80**, 1340–1342 (2002)
20. J.C. Simpson, J.F. Cordaro, Defect clusters in ZnO. J. Appl. Phys. **67**(11), 6760–6763 (1990)
21. J. Tanaka, S. Hishita, Deep levels near the grain boundary in a ZnO varistor: energy change due to electrical degradation. J. Am. Ceram. Soc. **73**, 1425–1428 (1990)
22. T.D. Chen, J.-R. Lee, H.L. Tuller and Y.-M.Chiang, Grain boundary dopants and heat treatment effects on the electrical properties of polycrystalline ZnO. in *Electrically Based Characterisation*, Mat. Res. Soc. Symp. Proc., ed. R.A. Gerhardt, S.R. Tylor and J. Garboczi (Material Research Society, Pittsburgh 1996) pp. 295–300
23. A. Tanaka, K. Mukae, ICTS measurements of single grain boundaries in ZnO: Rare-earth varistor. J. Electroceramics **4**(S1), 55–59 (1999)
24. A. Rohatgi, S.K. Pang, T.K. Gupta, W.D. Straub, The Deep Level Transient Spectroscopy Studies of a ZnO Varistor as a Function of Annealing. J. Appl. Phys. **63**(11), 5375–5379 (1988)
25. Y. Ohbuchi, J. Yoshino, Y. Okamoto, J. Morimoto, Evaluation of interface states in ZnO varistors by spectral analysis of DLTS. Jpn. J. Appl. Phys **38 Part1**(2A), 899–900 (1999)
26. Y. Ohbuchi, T. Kawahara, Y. Okamoto, J. Morimoto, The study of interface states in ZnO varistors by injection pulse width dependence of transient response. Jpn. J. Appl. Phys. **39 Part 1** (5A), 2665–2669 (2000)
27. Y. Ohbuchi, T. Kawahara, Y. Okamoto, J. Morimoto, Characterization of interface states in degraded ZnO varistors. Jpn. J. Appl. Phys. **41**, 190–196 (2002)
28. K. Mukae, A. Ohi, A. Tanaka, Electronic interface states at grain boundaries in ZnO: Pr varistors by single grain boundary measurements. J. Europ. Cer. Soc. **21**, 1871–1874 (2001)
29. J. Fan, R. Freer, Deep level transient spectroscopy of ZnO varistors doped with aluminium oxide and/or silver oxide. J. Am. Ceram. Soc. **77**, 2663–2668 (1994)
30. R.A. Winston, J.F. Cordaro, Grain-boundary interface electron traps in commercial ZnO varistors. J. Appl. Phys. **68**, 6495–6500 (1990)
31. D.V. Lang, Deep-level transient spectroscopy: A new method to characterize traps in semiconductors. J. Appl. Phys. **45**, 3023–3032 (1974)
32. D.K. Schroder, Semiconductor material and device characterisation (3rd edition) John Wiley & Sons Ltd, (2006)
33. P.R. Wilshaw, G.R. Booker, New results and an interpretation for SEM EBIC contrast arising from individual dislocations in silicon. Proceedings of the Microsc. Semicond. Mater. Conf. Oxford., 25–27 March Inst. Phys. Confr. Ser., **76,** 329–336 (1985)
34. P.N. Grillot, S.A. Ringel, E.A. Fitzgerald, G.P. Watson, Y.H. Xie, Electron trapping kinetics at dislocations in relaxed Ge0.3Si0.7/Si hetero-structures. J. Appl. Phys. **77**, 3248–3256 (1995)